Enhanced thermoelectric power factor of Bi2Sr2Co2Oy thin films by incorporating Au nanoparticles

Nian Fu, Liqing Sun, S. Liang, El Hadj Dogheche, Ahmed Addad, Shufang Wang

Materials and Design 89 (2016) 791–794

Enhanced thermoelectric power factor of $Bi_2Sr_2Co_2O_y$ thin films by incorporating Au nanoparticles

Nian Fu [a], Liqing Sun [a], S. Liang [b], Dogheche Elhadj [c], Ahmed Addad [d], Shufang Wang [a,*]

[a] Hebei Key Lab of Optic-electronic Information and Materials, The College of Physics Science and Technology, Hebei University, Baoding 071002, China
[b] Department of Chemistry, Renmin University of China, Beijing 100872, China
[c] University of Valenciennes & Hainaut Cambrèsis, Institute of Electronic Microelectronic Nanotechnology IEMN CNRS, Le Mont Houy, 59309 Valenciennes, France [d] UMET CNRS, Unité Matériaux et Transformations, Université Lille 1, 59655 Villeneuve d'Ascq, France

Article info

Keywords:
Thermoelectric
Layered cobaltite thin films
Au nanoparticles
Pulsed laser deposition

Abstract

c-Axis oriented $Bi_2Sr_2Co_2O_y$ thin films imbedded with Au nanoparticles were prepared by pulsed laser ablation a ceramic $Bi_2Sr_2Co_2O_y$ target with a small piece of Au foil overlapped. It was found that the incorporation of Au nanoparticles, about 5–15 nm in diameter, did not disrupt the *c*-axis orientation of the films. Fortunately, the incorporation of Au nanoparticles decreased the resistivity of $Bi_2Sr_2Co_2O_y$ films while maintained the Seebeck coefficient almost unchanged, thus resulted in an enhanced power factor. Possible mechanisms were proposed to explain the results. This work demonstrated a promising approach to optimize the thermoelectric performance of layered cobaltite thin films.

1. Introduction

Thermoelectric (TE) materials can convert thermal energy directly into electricity and vice versa, making them attractive for applications in waste heat recovery and Peltier cooling. The efficiency of thermoelectric materials is generally evaluated by the dimensionless figure of merit $ZT = (S^2/\rho\kappa)T$, where S, ρ, κ and T are Seebeck coefficient, electrical resistivity, thermal conductivity, and absolute temperature, respectively [1]. Therefore, the performance of TE materials can be enhanced by either increasing the power factor S^2/ρ or decreasing the thermal conductivity κ, which is the sum of the lattice and the carrier contribution.

Among all the TE materials explored, layered cobaltites have received increasing attention to the TE community in the past decade, particularly to those who are interested in high-temperature applications in air, because of their good TE performance, low cost, high thermal and chemical stability, and environmental benignity [2–4]. Various approaches were used to enhance the TE performance of the layered cobaltite bulks, such as improving the *c*-axis texture degree, optimizing the carrier concentration by doping, and introducing metallic nanoparticles (NPs) into the thermoelectric matrix [5–11]. *ZT* value of about 0.61 at 1118 K was reported for $Ca_3Co_4O_9$ polycrystalline bulks, a typical layered cobaltite, through ion doping and incorporating metallic Ag NPs into the TE matrix [11]. For localized heating or cooling, thin films are required in many particular applications. However, there are very few reports on the improvement of TE performance of thin film samples. In this work, we reported the enhancement of TE performance of thin films of layered cobaltite by incorporating metallic gold nanoparticles (Au NPs). *c*-Axis oriented $Bi_2Sr_2Co_2O_y$ (BSCO) thin films imbedded with Au NPs were fabricated on $LaAlO_3$ (001) single crystalline substrates by pulsed laser deposition (PLD) technique. By incorporating Au NPs into BSCO thin films, we found the power factor of the films was enhanced comparing to that of pure BSCO over a wide range of temperature. In addition, the thermal conductivity of the BSCO:Au NPs composite thin films was expected to decrease due to the enhanced phonon scattering on the Au NPs as well as the interface between the Au NPs and the BSCO TE matrix. Therefore, the TE performance of BSCO thin films could be improved by introducing Au NPs into the films.

2. Experimental

c-Axis oriented BSCO thin films imbedded with the Au NPs were fabricated on $LaAlO_3$ (001) single crystalline substrates by pulsed laser ablating a BSCO ceramic target, on which a piece of fan-shaped Au foil (99.99%) was attached. The distance between the target and the substrate was about 50 mm. An excimer laser with 308 nm radiation was used for the film deposition with a laser energy density of 1.5 J/cm^2 and a repetition rate of 3 Hz. The deposition temperature was monitored to be about 680 °C and the oxygen pressure in the PLD chamber was about 60 Pa. The Au concentration in the deposited BSCO films can be easily controlled by changing the area of Au foils. Three fan-shaped Au foils with $\omega = 0°$, 25° and 45° were used in this work

* Corresponding author.
E-mail address: swang2008@hotmail.com (S. Wang).

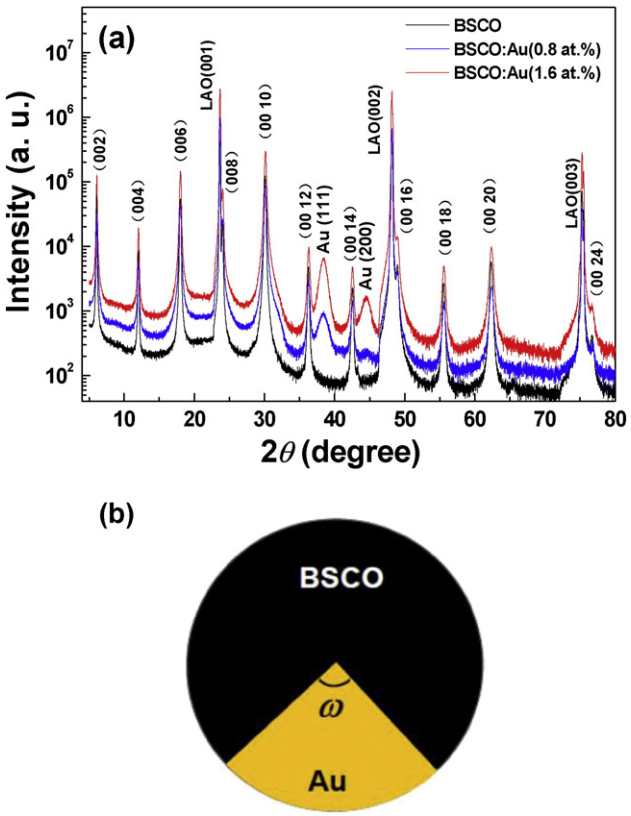

Fig. 1. (a) XRD θ-2θ scan of BSCO:Au composite thin films on $LaAlO_3$ (001) substrates. (b) The schematic image of BSCO:Au composite target.

(Fig. 1b), and the atomic ratio between Au and BSCO in the corresponding BSCO:Au composite films was about 0, 0.8 and 1.6%, respectively. It should be mentioned here that when we increased the Au atomic concentration to about 3.7% in the BSCO film (a fan-shaped Au foil with $\theta = 90°$ was used). The Seebeck coefficient of the resulting composite film decreased greatly, resulting in a reduction in TE performance.

The film thickness was measured by a Dektak 150 Surface Profiler and all film samples used in this work had thickness about 80 nm. The crystal structure of the films was identified by a Philips X'Pert 4-circle diffractometer with *CuKα* radiation. The Au concentration and chemical band in the composite films were determined by X-ray photoelectron spectroscopy (XPS) measurements. The microstructure were analyzed by a field-emission transmission electron microscopy (TEM, Tecnai G2 F20) equipped with an energy-dispersive X-ray spectroscopy (EDS) detector. The room temperature carrier concentration and mobility of the films was determined via Hall effect measurement by using a Physical Properties Measurement System (PPMS, Quantum Design Inc.). The temperature-dependent electrical resistivity and Seebeck coefficient were simultaneously measured using the dc four-probe method in Hall bar geometry by a LSR-3 measurement system (Linseis, Germany) with a heating rate of 5 K/min. To make the ohmic contact, silver paste was used for the terminal connections.

3. Results and discussion

Fig. 1a shows the typical XRD θ–2θ scans of the BSCO:Au composite thin films on $LaAlO_3$ (001) single crystalline substrates fabricated by pulsed laser ablation of the target. Schematic diagram of the target of BSCO with Au foil overlapped is shown in Fig. 1b. Except the diffraction peaks from the $LaAlO_3$ (LAO) and Au, all peaks in these three films can be indexed as 00ℓ diffractions from BSCO phase, suggesting that the resulting BSCO films are pure phase and *c*-axis oriented. As the concentration of Au in the films increases, the intensity of the Au diffraction peaks becomes stronger. In addition, the Au peaks also become broader, indicating that the size of Au particles in the films become smaller with the increase of the Au concentration. This might because that some small Au nanoparticles tend to agglomerate when the amount of Au in the films increases. We roughly estimate the average size of the Au particles in the films by the Au (111) peaks using the Scherer formula $D = (K\lambda)/(B\cos\theta)$, where D is the average size of the particles, K is the correction factor ($K = 0.89$), λ is the wavelength of X-ray ($\lambda = 0.15405$ nm), B is the full width at half maximum (FWHM) of Au (111) peaks shown in Fig. 1 and θ is the Bragg diffraction angle. The estimated D is about 5.4 and 8.0 nm for the films with the Au atomic concentration of 0.8 and 1.6%, respectively. We also estimated the number density of Au nanoparticles in these two films, which was about 4.94 and 8.02×10^{13}/cm^3, respectively.

Fig. 2a is the XPS survey spectra of a BSCO:Au composite thin film. It reveals that the cation ion ratio of Bi:Sr:Co in the film is about 1.00:1.03:1.06, which is very close to that of the nominal composition of this material. Moreover, the XPS measurement also reveals that the Au atomic concentration in this film is about 1.6%. Fig. 2b shows the Au 4f XPS core-level spectra of this film. The peaks of Au $4f_{5/2}$ and Au $4f_{7/2}$ are located at 87.6 and 84.0 eV, respectively, which correspond to the normal XPS spectra of metallic Au [12]. This result demonstrates that Au does not enter into the crystal lattice of BSCO but exists as a metallic phase in BSCO matrix.

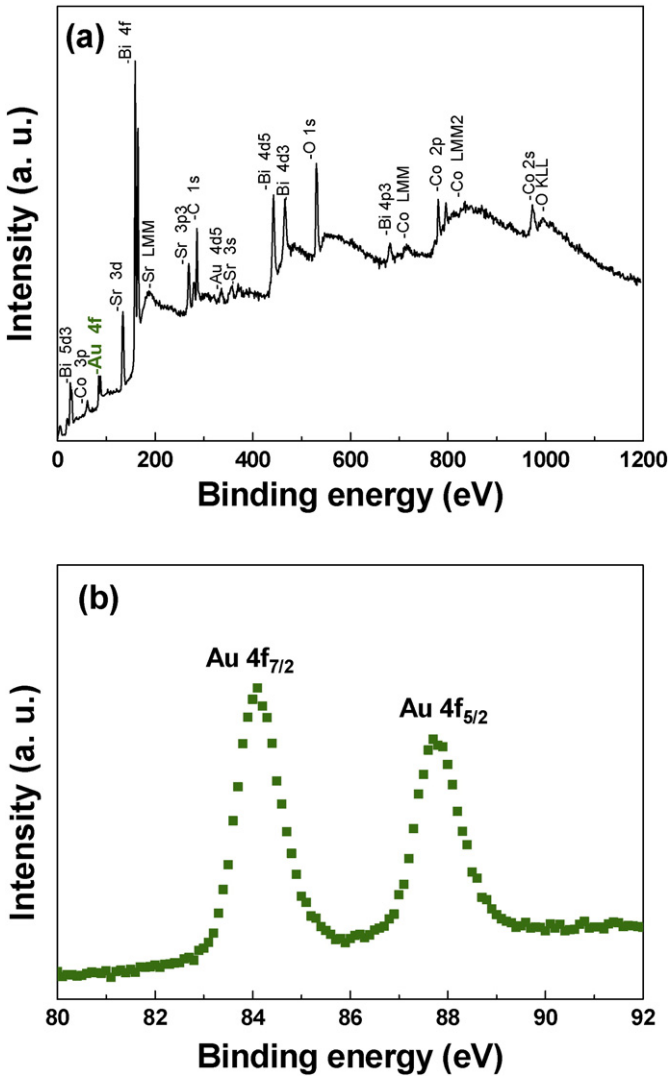

Fig. 2. (a) XPS spectra of BSCO:Au composite thin film with the Au atomic concentration of about 1.6%. (a) Survey scan and (b) high resolution core-level spectra of Au 4f.

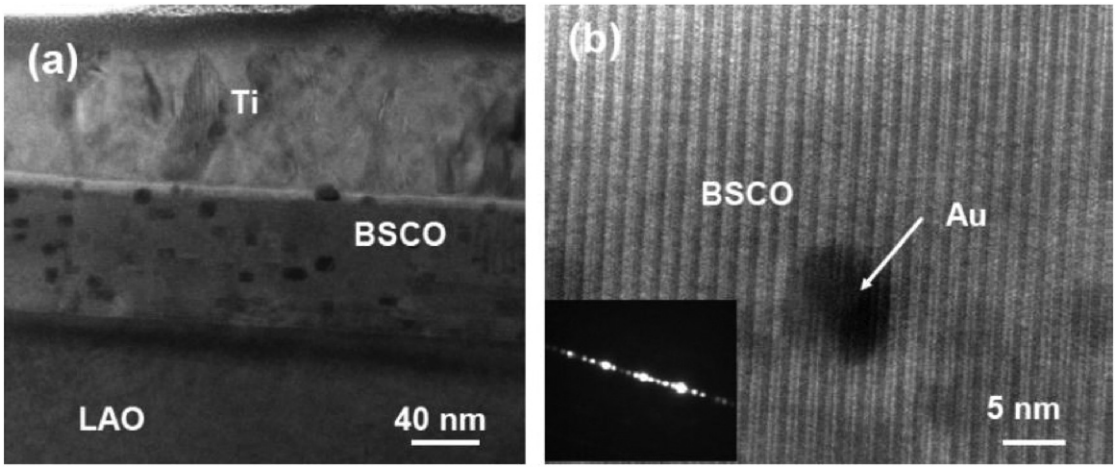

Fig. 3. (a) TEM and (b) HRTEM images of BSCO:Au composite thin film on $LaAlO_3$ (001) substrate. The inset of panel b is the SEAD pattern take form BSCO film area.

Fig. 3a shows the cross-sectional TEM micrography of the BSCO:Au composite film with the Au atomic concentration of about 1.6%. It can be seen that Au particles, having a diameter of about 5–15 nm, are well dispersed in the BSCO film matrix. Fig. 3b is the high-resolution TEM (HRTEM) micrography of the BSCO:Au composite film near the interface. Well-ordered layer structures of BSCO stacked along the *c* axis can be clearly observed and the introduction of Au NPs into the film does not disrupt the *c*-axis orientation growth of the film. The bright and dark stripes in the HRTEM image correspond to the conducting CoO_2 and insulating $Bi_2Sr_2O_4$ layers, respectively. Moreover, the selected area electron diffraction (SAED) pattern taken from the BSCO film area, shown in the inset of Fig. 3b, reveals that the film still maintains pretty good single crystallinity in spite of the Au addition.

The temperature dependence of in-plane electrical resistivity ρ_{ab} and Seebeck coefficient S_{ab} of these BSCO:Au composite thin films are shown in Fig. 4a and 4b, respectively. Both ρ and S increase when the temperature goes up, indicating a metallic conducting behavior. At the room temperature, the pure BSCO film has ρ and S of about 5 mΩ cm and 120 μV/K, leading to a high power factor of about 0.29 mW/K^2-m, which is comparable to that of single crystal bulks and is much higher than that of polycrystalline bulks [2,13–15]. Moreover, the incorporation of Au NPs into the BSCO film can decrease the resistivity of the films, and at the same time it has minor effect on the Seebeck coefficient. To better understand the effect of Au NPs on the resistivity and Seebeck coefficient, we measured the room temperature carrier concentration and mobility of these three films, which is shown in Table 1. It is somewhat surprising that incorporating Au NPs can increase the hole carrier concentration of BSCO films. A plausible explanation is that the Fermi level of Au is below the valence band edge of BSCO, and thus Au NPs can contribute holes to the BSCO film matrix due to the carrier transfer process. Similar effects have also been observed in other p-type semiconductor TE materials when incorporating metal or semimetal NPs into the semiconductor matrix [16–18]. In addition, Table 1 shows the carrier mobility of BSCO film does not change too much with Au addition, which indicates that the Au particles are too small to introduce charge carrier scattering [17]. In this case, we think that the reduction in the resistivity of BSCO film after introducing Au NPs is mainly caused by the increment in the hole carrier concentration of the film. Generally, the Seebeck coefficient S of a TE material decreases with the increment of carrier concentration. However, the S values of the present three films shown in Fig. 4b are almost the same, which might be due to the following two factors. First, the increase of carrier concentration induced by the addition of Au NPs leads to a decrease in Seebeck coefficient. Second, the metallic Au NPs could increase the energy dependent scattering

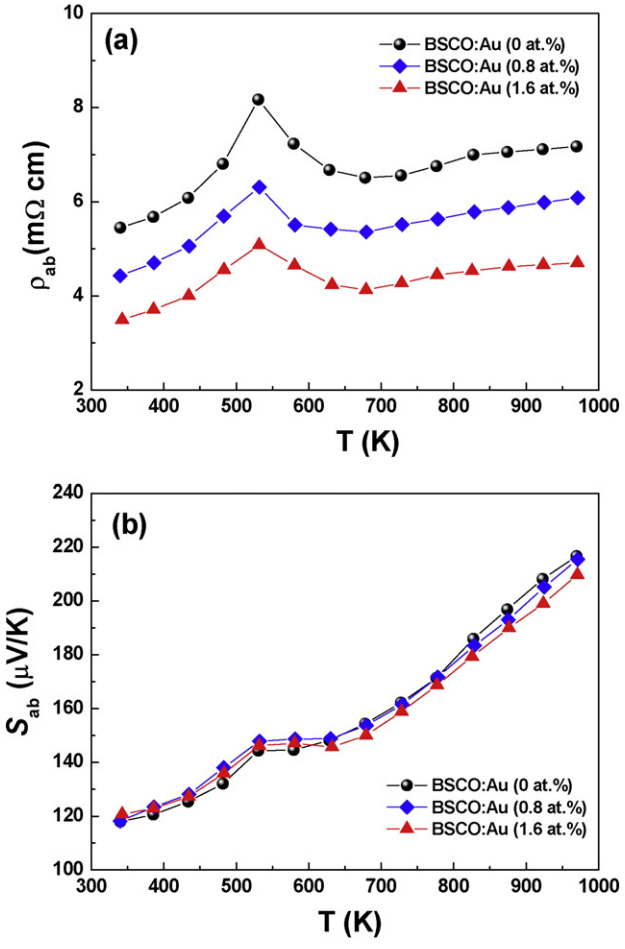

Fig. 4. (a) Temperature dependence of in-plane (a) resistivity ρ_{ab}, (b) Seebeck coefficient S_{ab} of BSCO:Au composite thin films.

Table 1
Room temperature carrier concentration n and Hall mobility μ of BSCO:Au composite thin films with different Au concentration x.

BSCO:Au (x at.%)	n (cm^{-3})	μ (cm^2/Vs)
0.0	5.61×10^{20}	2.13
0.8	6.26×10^{20}	2.24
1.6	8.82×10^{20}	2.31

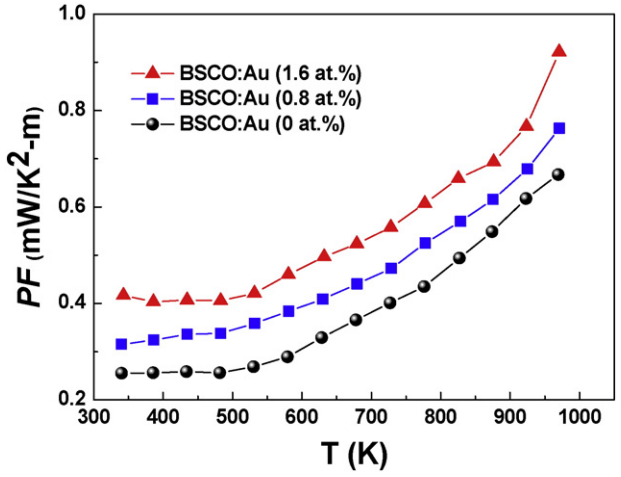

Fig. 5. Temperature dependence of in-plane power factor (*PF*) of BSCO:Au composite thin films.

time by preferentially tuning the scattering of carriers depending on their energy, leading to an enhancement in Seebeck coefficient [19–21].

We calculated the power factor of these three films at different temperatures, which is shown in Fig. 5. It can be seen that the addition Au NPs into BSCO films can increase the power factor of the films over the whole range of measured temperature. For example, the power factor of the BSCO:Au NPs (1.6 at.%) composite thin film is about 0.92 mW/K^2-m at 973 K, which is about 1.4 times higher than that of the pure film (~0.66 mW/K^2-m). Moreover, by introducing Au NPs of 5–15 nm in diameter into BSCO films, we believe that the thermal conductivity of the films could be lowered due to the enhanced scattering of the mid- and long-wavelength phonons at Au NPs and at the interfaces between the Au NPs and BSCO thin films [22–24]. Therefore, the *ZT* value of BSCO thin films is expected to significantly increase through incorporating Au NPs into the films.

4. Conclusion

Pure phase, *c*-axis oriented BSCO thin films imbedded with Au NPs, having a diameter of about 5–15 nm, were fabricated on $LaAlO_3$ (001) single crystalline substrates by pulsed laser deposition technique. It was found that the incorporation of Au NPs into BSCO films can improve the electrical conductivity of the films while without deteriorating the Seebeck coefficient, resulting in an enhancement in power factor. Moreover, the presence of Au NPs might provide scattering centers for phonons, leading to a decrease in thermal conductivity. Due to enhanced power factor and decreased thermal conductivity, the figure of merit, *ZT*, could improve accordingly.

Acknowledgments

This work is supported by the National Nature Science Foundation of China (Grant No. 51372064), the Nature Science Foundation for Distinguished Young Scholars of Hebei Province (Grant No. A2013201249) and the One Hundred Talent Project of Hebei Province (Grant No. E2013100013).

References

[1] H.J. Goldsmid, in: D.M. Rowe (Ed.), Chapter 3:Conversion Efficiency and Figure-of-Merit, CRC Handbook of Thermoelectrics, CRC Press, 1995.
[2] K. Koumoto, I. Terasaki, R. Funahashi, MRS Bull. 31 (2006) 206.
[3] M. Lee, L. Viciu, L. Li, Y.Y. Wang, M.L. Foo, S. Watauchi, R.A. Pascal Jr., R.J. Cava, N.P. Ong, Nat. Mater. 5 (2006) 537.
[4] R. Funahashi, M. Shikano, Appl. Phys. Lett. 81 (2002) 1459.
[5] Y. Wang, Y. Sui, P. Ren, L. Wang, X.J. Wang, W.H. Su, H.J. Fan, Chem. Mater. 22 (2010) 1155.
[6] C.-J. Liu, L.-C. Huang, J.-S. Wang, Appl. Phys. Lett. 89 (2006) 204102.
[7] R.H. Wei, X.W. Tang, Z.Z. Hui, J. Yang, L. Hu, L. Chen, J.M. Dai, X.B. Zhu, Y.P. Sun, J. Amer. Ceram. Soc. 97 (2014) 1841.
[8] S.F. Wang, Z.C. Zhang, L.P. He, M.J. Chen, W. Yu, G.S. Fu, Appl. Phys. Lett. 94 (2009) 162108.
[9] X.B. Zhu, D.Q. Shi, S.X. Dou, Y.P. Sun, Q. Li, L. Wang, W.X. Li, W.K. Yeoh, R.K. Zheng, Z.X. Chen, C.X. Kong, Acta Mater. 58 (2010) 4281.
[10] T. Motohashi, Y. Nonaka, K. Sakai, M. Karppinen, H. Yamauchi, J. Appl. Phys. 103 (2008) 033705.
[11] N.V. Nong, N. Pryds, S. Linderoth, M. Ohtaki, Adv. Mater. 23 (2011) 2484–2490.
[12] M.P. Seah, I.S. Gilmore, G. Beamson, Surf. Interface Anal. 26 (1998) 642.
[13] R. Funahashi, I. Matsubara, S. Sodeoka, Appl. Phys. Lett. 24 (2000) 2385.
[14] H.C. Hsu, W.L. Lee, K.K. Wu, Y.K. Kuo, B.H. Chen, F.C. Chou, J. Appl. Phys. 111 (2012) 103709.
[15] G.J. Xu, R. Funahashi, M. Shikano, I. Matsubara, Y.Q. Zhou, J. Appl. Phys. 91 (2002) 4344.
[16] D.-K. Ko, Y.-J. Kang, C.B. Murray, Nano Lett. 11 (2011) 2841.
[17] I.-H. Kim, S.-M. Choi, W.-S. Seo, D.-I. Cheong, Nanoscale Res. Lett. 7 (2012) 2.
[18] H. Lu, P.G. Burke, A.C. Gossard, G. Zeng, A.T. Ramu, J.-H. Bahk, J.E. Bowers, Adv. Mater. 23 (2011) 2377.
[19] J.P. Heremans, C.M. Thrush, D.T. Morelli, J. Appl. Phys. 98 (2005) 063703.
[20] B. Paul, A. Kumar, V.P. Banerji, J. Appl. Phys. 108 (2010) 064322.
[21] X.H. Yang, X.Y. Qin, Appl. Phys. Lett. 97 (2010) 192101.
[22] T.S. Basu, R.G. Yang, S.J. Thiagarajan, S. Ghosh, S. Gierlotka, M. Ray, Appl. Phys. Lett. 103 (2013) 083115.
[23] M.V. Warren, J.C. Canniff, H. Chi, E. Morag, F. Naab, V.A. Stoica, R. Clarke, C. Uher, R.S. Goldman, J. Appl. Phys. 114 (2013) 043704.
[24] M. Koirala, H.Z. Zhao, M. Pokharel, S. Chen, T. Dahal, C. Opeil, G. Chen, Z.F. Ren, Appl. Phys. Lett. 102 (2013) 213111.